LANGMUIR

Interface Components: Nanoparticles, Colloids, Emulsions, Surfactants, Proteins, Polymers

Kinetically Stable Triglyceride-Based Nanodroplets and Their Interactions with Lipid-Specific Proteins

Valerija Vezo#nik, Vesna Hodnik, Simona Sitar, Halil I. Okur, Magda Tušek Žnidari#, Cornelis Lütgebaucks, Kristina Sep#i#, Ksenija Kogej, Sylvie Roke, Ema Žagar, and Peter Macek

Langmuir, **Just Accepted Manuscript** • DOI: 10.1021/acs.langmuir.8b02180 • Publication Date (Web): 07 Jul 2018

is published by the American Chemical Society. 1155 Sixteenth Street N.W., Washington, DC 20036

Kinetically Stable Triglyceride-Based Nanodroplets and Their Interactions with Lipid-Specific Proteins

Valerija Vezočnik, [†] *Vesna Hodnik,* [†] *Simona Sitar,* [‡] *Halil I. Okur,* [‖] *Magda Tušek-Žnidarič,* [§] *Cornelis Lütgebaucks,* [‖] *Kristina Sepčić,* [†] *Ksenija Kogej,* [#] *Sylvie Roke,* [‖] *Ema Žagar,* [‡]

and Peter Maček[*, †]

[†]Department of Biology, Biotechnical Faculty, University of Ljubljana, Jamnikarjeva 101, Ljubljana, 1000, Slovenia

[‡] Department of Polymer Chemistry and Technology, National Institute of Chemistry, Hajdrihova 19, Ljubljana, 1000, Slovenia

[‖]Laboratory for Fundamental BioPhotonics, Institute of Bio-Engineering, and Institute of Material Science, School of Engineering , and Lausanne Centre for Ultrafast Science, École Polytechnique Fédérale de Lausanne, CH-1015 Lausanne, Switzerland

[§]National Institute of Biology, Večna pot 111, Ljubljana, 1000, Slovenia

[#]Department of Chemistry and Biochemistry, Faculty of Chemistry and Chemical Technology, University of Ljubljana, Večna pot 113, Ljubljana, 1000, Slovenia

KEYWORDS: cholesterol, equinatoxin II, oil-in-water emulsion, lipid droplets, nanoemulsion, perfringolysin O, sphingomyelin.

ABSTRACT

Understanding of the interactions between proteins and natural and artificially prepared lipid membrane surfaces and embedded non-polar cores is important in studies of physiological processes and their pathologies, and is applicable to nanotechnologies. In particular, rapidly growing interest in cellular droplets defines the need for simplified biomimetic lipid model systems to overcome *in vivo* complexity and variability. We present a protocol for preparation of kinetically stable nanoemulsions with nanodroplets composed of sphingomyelin (SM) and cholesterol (Chol), as amphiphilic surfactants, and trioleoylglycerol (TOG), at various molar ratios. To prepare stable SM/Chol-coated monodisperse lipid nanodroplets, we modified a reverse phase evaporation method and combined it with ultra-sonication. Lipid composition, ζ-potential, gyration and hydrodynamic radius, shape, and temporal stability of the lipid nanodroplets were characterized, and compared to extruded SM/Chol large unilamellar vesicles. Lipid nanodroplets and large unilamellar vesicles with theoretical SM/Chol/TOG molar ratios of 1/1/4.7 and 4/1/11.7 were further characterized. Their orientational order of their interfacial water molecules was defined using a second harmonic scattering technique, along with their interactions with the SM-binding and Chol-binding pore-forming toxins equinatoxin II and perfringolysin O, respectively. The surface characteristics (ζ-potential, orientational order of interfacial water molecules), and binding of these proteins to the nanodroplet SM/Chol monolayers were similar to those for the SM/Chol bilayers of the large unilamellar vesicles and SM/Chol Langmuir monolayers, in terms of their surface structures. We propose that such SM/Chol/TOG nanoparticles with the required lipid compositions can serve as experimental models for monolayer membrane to provide a system that imitates the natural lipid droplets.

INTRODUCTION

Chylomicrons, plasma lipoproteins, milk fat globules, and intracellular lipid droplets have the form of oily droplets that contain triacylglycerols and cholesteryl esters that are surrounded by a monolayer of amphiphilic phospholipids and cholesterol, including specific proteins.[1-3] These particles can be biophysically modelled as oil-in-water emulsion droplets.[4-5] In particular, plasma lipoproteins and cellular lipid droplets have inspired researchers to develop simplified biomimetic nanostructures as cargo delivery systems, or for model systems in biophysical and biochemical research.[6-13]

The chemical characteristics of amphiphilic lipids and their spatial organization within the monolayer that cover the non-polar lipid droplets will govern the first-line interactions of these lipid droplets with other biomolecules, such as proteins dissolved in the water phase. A plethora of reports on standard models of lipid bilayers and monolayers (Langmuir monolayers) and their interactions with proteins have been published to date as reviewed in[14-18]. In contrast, similar studies on artificial lipid droplets are scarce, although proteins might interact with the lipid monolayer of lipid droplets in a similar manner to their interactions with lipid Langmuir monolayers or planar bilayer membranes. To test this idea, we developed a simple and cost-effective protocol for the preparation of nanoemulsion-based lipid nanodroplets (LDs) using a modified reverse-phase evaporation method combined with ultra-sonication. Here, we chose sphingomyelin (SM) and cholesterol (Chol) as surfactants, both of which are found in plasma lipoproteins and cellular lipid droplets[19-21], and trioleoylglycerol (TOG) as the in-water dispersed phase. The mixed SM and Chol are of particular interest, because they might form the liquid ordered phase, *l*o, that is fundamental for promotion of specific membrane domains, such as lipid

rafts.[22-24] We then analyzed these nanoemulsion nanodroplets in terms of their lipid composition, size, polydispersity, and stability. We examined their surface thorough measurement of their ζ-potential, and we took advantage of a second harmonic scattering technique[25-27] to characterize the orientational order of their interfacial water molecules. Finally, we probed the nanodroplet surface for the binding of SM-specific and Chol-specific proteins, compared to SM/Chol large unilamellar vesicles (LUVs) and Langmuir monolayers.

Our data indicate that in addition to standard well-established lipid membrane models, these kinetically stable SM/Chol/TOG nanodroplets can serve as a biomimetic lipid system for experimental studies. Moreover, these artificial nanodroplets can be used as a surrogate in detailed biophysical and biochemical studies of more complex cellular lipid droplets.

EXPERIMENTAL SECTION

Chemicals and Buffers. Daily fresh stock solutions of each single lipid were prepared in chloroform by dissolving the TOG (≥ 99 %; M_r = 885.4; Sigma-Aldrich, Munich, Germany) or wool grass Chol (> 98 %; M_r = 386.4; Avanti Polar Lipids, Alabaster, U.S.A), while porcine brain SM (> 99 %; mean M_r = 760.2; Avanti Polar Lipids, Alabaster, U.S.A) was dissolved in chloroform/ methanol (20/1, v/v). The recombinant SM-specific actinoporin, EqTx II (PDB: 1IAZ) was prepared and characterized as described previously.[28] The recombinant Chol-dependent cytolysin, PFO (PDB: 1PFO_A), that lacked the N-terminal signal peptide of 28 amino acids, was a generous gift from S. Rezelj and G. Anderluh (National Institute of Chemistry, Ljubljana, Slovenia). Bovine serum albumin was from Sigma-Aldrich (Munich, Germany). All other chemicals used were of analytical grade and were used as received (from

Sigma-Aldrich, Munich, Germany). Chloroform and methanol were from Carlo Erba Reagents (Val-de-Reuil, France), and nitrogen gas (N_2 (g)) from Messer Slovenia (Ljubljana, Slovenia). Solutions were prepared using Milli-Q water. LDs and LUVs were prepared in 140 mM NaCl/ 20 mM Tris.HCl/ 1 mM EDTA, pH 7.4 (Buffer A). For measurements of zeta-potential of LDs and LUVs, 5 mM Tris.HCl/ 0.25 mM EDTA, pH 7.4 (Buffer B) was used. SHS measurements were performed in 100 μM Tris.HCl/ 25 μM EDTA, pH 7.4 (Buffer C).

Preparation of unilamellar vesicles and nanoemulsion lipid nanodroplets. In step 1, which was common to the preparation of LDs and LUVs, SM, Chol and TOG (LDs), or SM and Chol (LUVs), were dispersed in the Buffer A. To make lipid dispersions, we had developed a modified reverse-phase evaporation method. A two-phase system was prepared: the lower phase included the dissolved lipids in chloroform, and the upper phase was Buffer A. Instead of the usual removal of lipid solvents under vacuum[29-30], the lower solvent phase was removed by purging it with a stream of N_2 (g). In the second step using the respective lipids dispersions, nanoemulsions of LDs were produced by ultra-sonication and centrifugation, while LUVs were prepared by the extrusion method (for details, see **Supporting Information, Preparation of lipid vesicles and LDs, Scheme S1)**.

Lipids concentration determination. The contents of TOG, SM, and Chol in the final LD and LUV preparations were determined colorimetrically (Wako test triglyceride kit; Wako test phospholipids C kit; Wako test free cholesterol E kit; Wako Chemicals GmbH, Neuss, Germany).

Dynamic light scattering (LDS). The DLS measurements were conducted using a three-dimensional cross-correlation spectrometer (LS Instruments GmbH, Fribourg, Switzerland). The DLS measurements were performed in cylindrical quartz cuvettes at 25 °C, using a He-Ne laser

with a wavelength of 633 nm. Each sample was thermostated for 15 min before five repeat measurements were performed. The fluctuations in the intensity of the scattered light were monitored at an angle of 90°. The hydrodynamic radii of the particles, R_h, were determined using CONTIN analysis.[31] Polydispersity was calculated from the first and second cumulants as reported in detail previously.[32-33]

The z-average hydrodynamic radius (R_h) and polydispersity (PI) of samples were determined using a Zetasizer Nano ZS ZEN 3600 (4 mW He–Ne laser, 633 nm) from Malvern Instruments (Malvern, UK). Scattered light was detected at 173° by the automatically adjusted laser attenuation filters and the measurement position within the cell at 25 °C. For the evaluation of R_h, the viscosity of 0.8863 mPa (at 25 °C) and the refractive index of 1.339 (at 633 nm) were used for buffer solutions.

ζ-potential measurement. A Zetasizer Nano ZS ZEN 3600 (Malvern Instruments Ltd., Worcestershire, UK) was used for electrokinetic mobility measurements, to determine the particles ζ-potential. The LDs and LUVs were diluted in Buffer B (1 : 25, v/v) and monitored for pH with a microelectrode, before the measurements that weres conducted in disposable folded capillary cells (CTS1070; Malvern Instruments Ltd., Worcestershire, U.K.), at 25 °C.

Asymmetrical flow field flow fractionation (AF4). The AF4 separations were performed using an Eclipse3+ system (Wyatt Technology Europe GmbH, Dernbach, Germany) connected to an isocratic pump, an on-line vacuum degasser, and an auto-sampler (Agilent 1260 series; Agilent Technologies, Santa Clara, USA) as described previously in detail[34-35] while the running eluent was Buffer A (140 mM NaCl, 20 mM Tris-HCl, 1 mM EDTA, pH 7.4). The sizes of the LDs and LUVs were expressed as the radii of gyration, R_g, determined by the multi-angle-light-scattering (MALS) detector, without the need for solute concentration and sample refractive

index increment. The R_g radii of the fractionated samples were calculated using the data from 15 angles from the MALS, applying a second-order Zimm approximation for LDs, and a second-order Debye approximation for LUVs.

Second harmonic scattering (SHS). The SHS measurements were performed with the experimental set-up and measurement protocols described elsewhere.[10, 12] Briefly, a 190-fs, 1028-nm laser with a 200-kHz repetition rate was used as the fundamental input beam. The polarization of the input beam was controlled by a Glan-Taylor polarizer (GT10-B, Thorlabs) and a zero-order half wave plate (WPH05M-1030). The incoming beam with 0.3 μJ pulse energy was also filtered with a FEL0750 filter (Thorlabs). The input beam was then focused into a cylindrical glass cuvette with an inner diameter of 4.2 mm. The focus had a waist diameter of ~35 μm and a Rayleigh length of 0.94 mm. The scattered SH beam generated was analyzed (GT10-A, Thorlabs), filtered with a notch filter (ET525/50, Chroma), collimated with a plano-convex lens (f = 5 cm), and finally focused into a gated photomultiplier tube (H7421-40; Hamamatsu). The data points were recorded with 20 × 1 s acquisition time and a gate width of 10 ns. The detection angle (that had an acceptance angle of 11.4°) was set to a scattering angle θ_{max} that corresponded to the angle of maximum intensity. The reproducibility of the SHS measurement was in the range of 1% to 2%. The SHS intensity was corrected for background hyper Rayleigh scattering, which was normalized to that of 18.1-MΩ.cm water, recorded in the PPP-polarization combination:

$$S(\theta) = \frac{I(\theta_{max})_{SHS,droplets,PPP} - I(\theta_{max})_{HRS,solution,PPP}}{I(\theta_{max})_{HRS,water,ppp}}.$$

The SHS signal was normalized by the particle size, taking an effective radius R_h obtained from the DLS size distribution as described previously.[27] Thus, the data presented reports on the size normalized scattering of a single nanodroplet.

Surface plasmon resonance measurements (SPR). The interactions between LDs or LUVs immobilized onto a sensor chip and EqTx II or PFO were studied using a Biacore X system (Biacore, Uppsala, Sweden). In each experimentation cycle, a sensor L1-chip (Biacore, Uppsala, Sweden) was equilibrated in Buffer A. After a 1-min pulse of aqueous 0.5% sodium dodecyl sulfate at the flow rate of 10 μL/min, the lipid particles were captured on the surface of the L1 chip. The LDs and LUVs were immobilized at concentrations of 0.07 mg/mL and 0.7 mg/mL total lipid, respectively, for 10 min, at a flow rate of 2 μL/min. A 1-min pulse of 0.1 mg/mL bovine serum albumin at the flow rate of 10 μL/min blocked the remaining non-specific binding surface, and fully covered the L1 chip surface. When the SPR response was stable, a solution of 50 nM EqTx II or 500 nM PFO was injected for 60 s, followed by a 180-s dissociation period, at a flow rate of 10 μL/min. The cycle was completed by chip regeneration with a 1 min pulse of 0.5% sodium dodecyl sulfate at the flow rate of 10 μL/min, followed by two 1-min pulses of 40 mM octyl-D-glucoside at a flow rate of 100 μL/min and 10 μL/min. Finally, a 1-min pulse of 70% ethanol at a flow rate of 10 μL/min was used to wash the microfluid system. The results of blank injections were subtracted from the sensorgrams to correct for the contribution of the buffer.

Langmuir monolayers. The **s**urface pressure of the lipid monolayers was determined using a MicroTrough-S system (Kibron, Helsinki, Finland) at room temperature under constant stirring. The aqueous sub-phase was 450 μL of Buffer B. SM/Chol of 1/1 and 4/1 (mole/mole) lipid mixtures were dissolved in chloroform/methanol (20/1, v/v) and gently spread over the sub-phase to create a lipid monolayer. After a 10-min incubation, 500 nM PFO was injected through a hole connected to the sub-phase. The increment in the surface pressure *vs*. time was monitored for at least 30 min.

Transmission electron microscop (TEM). Lipid structures were visualized using an electron microscope (Philips CM 100; FEI, Eindhoven, Netherlands) operating at 80 kV. The LDs 1/1 or LUVs 1/1 in Buffer A were mixed with PFO at a Chol/PFO molar ratio of 200/1. After a 15-min incubation, 3 μL of sample was left on a formvar and carbon-coated copper grid for 60 s. Langmuir monolayers were transferred directly from the wells by touching the top of the in-well meniscus with a formvar and carbon-coated copper grid. Three droplets of deionized water were adhered to the grid for 1 s to 2 s to reduce salt effects. Excess solution was removed with Whatman filter paper, and the samples were negatively stained with 1% (w/v) uranyl acetate, with the excess staining solution blotted and the grid allowed to dry. The data were collected with a CCD camera (Orius SC 200; Gatan Inc., Pleasanton, USA) using the Digital Micrograph Software (Gatan Inc., Pleasanton, USA).

RESULTS AND DISCUSSION

Here, we addressed two main questions: whether the combination of SM and Chol can stabilize nanoemulsion-based TOG nanodroplets, and whether the surface characteristics of the SM/Chol monolayer of the nanodroplets are similar to those of SM/Chol bilayers of LUVs and SM/Chol Langmuir monolayers, in terms of the surface structure and the interactions with proteins that bind specifically to either SM or Chol. To answer these questions we first examined the ζ-potential, and the orientational order of the interfacial water molecules around these nanodroplets and around LUVs. Secondly, we made use of perfringolysin O (PFO), a proto-type of Chol-dependent cytolysins[36-40] and equinatoxin II (EqTx II), a SM-binding actinoporin.[41] As these two proteins have been demonstrated to selectively interact with cholesterol-rich

membrane surfaces and with sphingomyelin, respectively[42], we used them to probe the nanodroplet surface.

Preparation of nanodroplets. The preparation of nanoemulsions composed of amphiphilic lipids and triacylglycerols in water can be started by conventional rehydration and mechanical dispersion into the water phase of the dried lipid mixture as used for the preparation of lipid vesicles.[43] However, this first step has the disadvantage that due to sticking of the liquid triacylglycerols to glass or plastic materials, the final preparations can show poor lipid recovery, which can introduce significant discrepancy between the theoretical and actual lipid composition.[7, 34-35] Moreover, another drawback of this method arises from the solubility limit of cholesterol in phospholipids and its micro-crystallization, which is also dependent on the method of preparation of hydrated lipid films. Consequently, the inclusion of Chol into hydrated films cannot be defined with any precision.[44] Therefore, here, we modified the original reverse-phase evaporation method[45] to prepare initial lipid dispersions that were further processed by extrusion or ultra-sonication. Distinct from the original method, instead of applying a vacuum, we purged the mixed organic solvent and water phases with gaseous nitrogen, to remove the lipid solvents, and thus to obtain SM/Chol and SM/Chol/TOG dispersions, while also preventing lipid oxidation. In the next step, the extruded LUVs and ultra-sonicated small unilamellar vesicles (SUVs) or LDs were obtained and characterized.

Characterization of nanodroplets. All of the lipid preparations were first analyzed colorimetrically, to define their SM/Chol/TOG molar ratio and levels of any residual chloroform. Indeed, a drawback of this reverse-phase evaporation method can be the retention of residual organic solvents[44] However, this analysis showed the residual chloroform to be below 0.2 ppb in the final lipid dispersions.

The fixed parameters in the nanodroplets preparation are their composition and ionic strength, the pH and composition of the preparation buffer (Buffer A; see EXPERIMENTAL SECTION), the preparation temperature (60 °C) relative to the melting temperature of SM/Chol mixtures (41 °C)[46], and the low total lipid concentration in Buffer A. Therefore, the stability of nanoemulsions produced will be mainly dependent on the nanodroplet surface properties (e.g. charge) and size, and the interfacial properties of an oil-in-water emulsion, which will affect colloidal interactions.[47-48] Here, the nanodroplets size will be dependent on the work input (i.e., power and time of ultra-sonication) for the SM/Chol/TOG dispersions. On this basis, using the fixed theoretical (nominal) ratio of SM/Chol of 1/1 or 4/1, we first studied the effects of varied theoretical (SM + Chol)/TOG molar ratios on the on final lipid composition and the ζ-potential, size and size distribution of the nanodroplets using successive ultra-sonication and centrifugation (**Table 1** and **Table 2**; **Supporting Information, Figure S1**, **Table S1**).

It was evident that the experimentally determined final molar ratios of (SM + Chol)/TOG in the isolated LDs differed from the initial theoretical ratios used for the dispersion preparations. In particular, the molar fraction of Chol determined for the LDs systematically exceeded the theoretical SM/Chol molar ratio of 4/1 (**Table 1**). Critical consideration of the SM/Chol/TOG molar ratios determined (**Table 1**) for the 1/1 and 4/1 LDs (**Table 2**) in terms of their estimated sizes suggests that the data also deviated from the theoretically derived surface/core mass ratios (i.e., (SM + Chol)/TOG) for ideal spherical lipid droplets of defined geometric radius, *R* (for details, see **Supporting Information, Figure S2**). Similarly, a surplus of amphiphilic surfactants over TOG was previously reported for phosphatidylcholine/Chol/TOG LDs.[7] This observed surplus of (SM + Chol) over TOG might be accounted for by the presence of SUVs and (multi)lamellar SM/Chol structures formed from SM and Chol in excess over TOG, as reported

previously for phospholipid/oil nanoemulsions.[49] Alternatively, the observed excess Chol content might derive from greater solubility of Chol in the triacylglycerol core compared to SM, and be related to a larger volume of the TOG core in comparison to the surface monolayer of the LDs, as reported previously.[6-7, 50] Nevertheless, based on previous studies[7, 34, 49] and the present study we believe that the reduction in the amphiphilic lipids to 20 to 30 mole-% is not beneficial as the initial theoretical (SM + Chol)/TOG molar ratios of around 0.7 provided the lowest nanoemulsion polydispersity and the highest lipid recovery. When the TOG content exceeded ~80 mole%, the LDs were polydispersed with bimodal or multimodal size distributions, and they showed increased tendency to coalesce and aggregate. Meanwhile, decreasing TOG below ~50 mole% led to the formation of unstable mixtures of SUVs, of nanodroplets shielded with multiple lamellae, and of LDs with a wide size distribution, as was also shown here by transmission electron microscopy (TEM; data not shown). Based on these data, we focused on the LDs with constant theoretical 70 mole% TOG at varied SM/Chol ratios, as the SM/Chol/TOG molar ratio of 1/1/4.7 (designated as LDs 1/1) and 4/1/11.7 (LDs 4/1).

Effects of lipid composition on nanodroplet ζ-potential. In initial experiments, variation of the LDs SM/Chol/TOG molar ratio of the LDs revealed that the negative ζ-potential of both the pure TOG nanodroplets, of about -77 mV, and the Chol/TOG nanodroplets, of about -65 mV (**Figure 1A**), could be "titrated" by gradually increasing the SM molar fraction, as shown in **Figure 1B.** The markedly negative ζ-potential here for the pure TOG nanodroplets with a non-polar surface is in agreement with previous reports on the ζ-potential and surface electric potential of non-polar oil/water interfaces.[25, 51-52] Increasing the Chol molar fraction above about 0.1 in the Chol/TOG nanodroplets reduced their negative ζ-potential to about -65 mV (**Figure 1B,** inset). It appears that the membrane-bound Chol can only slightly modulate the ζ-potential

of the LDs, as reported before for extruded vesicles.[53] In this previous study[53], gradual inclusion of up to 50 mole% Chol into phosphatidylcholine vesicles changed their ζ-potential from +2 mV to -5 mV, which are close to those for the extruded SM/Chol LUVs and sonicated SM/Chol SUVs (**Supporting Information, Table S1**; **Table 2**). Gradually increasing the molar fraction of SM in the LDs decreased their negative ζ-potential, which reflected changes in the surface electrical properties of the LDs. As shown in **Figure 1B,** at a molar fraction of SM above about 0.1, the ζ-potential reached "saturation" at about -4.5 to -9 mV, which is comparable to about -2 mV to -6 mV as measured for the SM/Chol vesicles. The integrity, shape, and size of the lipid particles examined were monitored by TEM, as shown in **Figure 1C**.

Table 1. Colorimetric determination of SM, Chol, and TOG content in the LD and LUV preparations. Designations 1/1 and 4/1 are theoretical molar ratios of SM and Chol. Colorimetric data are means ±standard deviations from 10 independent preparations.

Lipid preparation	SM	Chol	TOG	Total lipid recovery (weight-%)
LDs 1/1	16 ± 3	14 ± 2	70 ± 4	60 – 75
LDs 4/1	20 ± 3	8 ± 2	72 ± 4	60 – 75
LUVs 1/1	52 ± 4	48 ± 4	0	40 – 55
LUVs 4/1	78 ± 4	22 ± 4	0	40 – 55

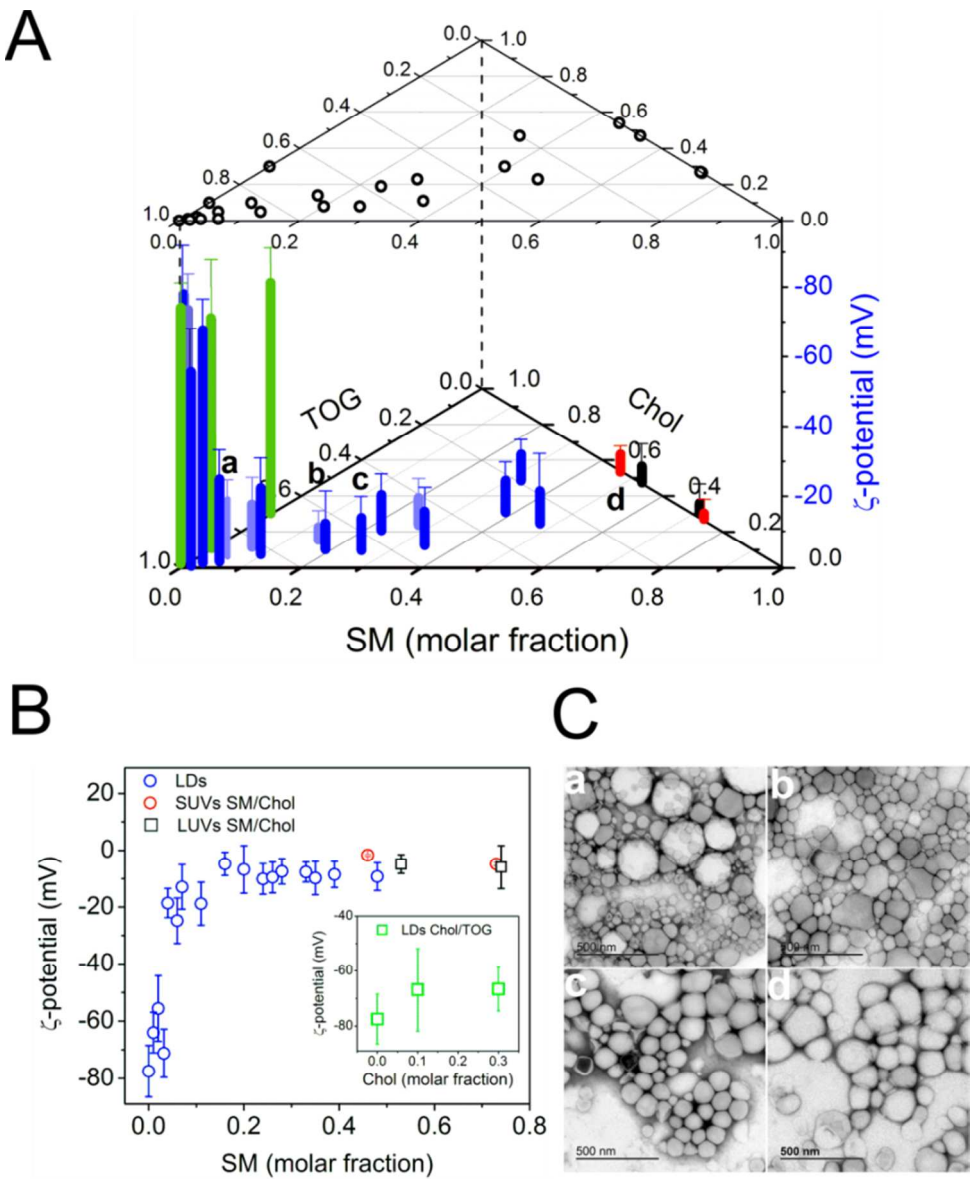

Figure 1. Effects of lipid composition on ζ-potential of lipid nanodroplets (LDs) and sphingomyelin/cholesterol (SM/Chol) large (LUVs) and small (SUVs) unilamellar vesicles. (A) Three-dimensional representation depicting the varied molar fractions SM, Chol, and trioleoylglycerol (TOG) in LDs (blue), LUVs (black), and SUVs (red), and their corresponding ζ-potentials. Colored data bars present mean ζ-potential ± ζ-deviation (n = 3). (B) Dependency of ζ-potential on SM molar fraction for LDs, LUVs, and SUVs. Inset: Effects of Chol molar

fraction on ζ-potential of Chol/TOG LDs (green). Data are means ±standard deviations (n = 5) (C) Representative TEM images of particles, corresponding to letters given in panel (A): (a) LDs (SM/Chol/TOG 6/1/93); (b) LDs (SM/Chol/TOG 20/8/72); (c) LDs (SM/Chol/TOG 26/8/66); (d) SUVs (SM/Chol 46/54). Lipid compositions of LDs and vesicles were determined colorimetrically.

Characterization of LDs 1/1 and LDs 4/1. The size of the droplets is important for the kinetic stability of nanoemulsions. Decreased droplet size reduces the rate of coalescence, aggregation, and gravitational separation of oil-in-water emulsions.[48, 54] To this end, we examined the time of ultra-sonication at a constant operating power that was necessary to reach the lower limit of sizes for the LDs 1/1 and LDs 4/1 (**Figure 2**). For all of the investigated LDs, 10 min to 15 min of ultra-sonication was sufficient to reach their lowest constant hydrodynamic radius, of $R_h \leq 80$ nm, and polydispersity, of ≤ 0.15, as estimated by DLS. In comparison, the SM/Chol/TOG dispersions obtained by the modified reverse-phase evaporation method and before ultra-sonication, (see **Supporting Information, Scheme S1**) had R_h around 500 nm. The time-course and duration of ultra-sonication that were needed to produce the minimal size of nanodroplets defined here (**Figure 2**) are very similar to those reported by Delmas *et al*.[54]. Therefore, 15-min ultra-sonication was applied for all of the preparations of the LDs 1/1 and LDs 4/1, which resulted in monomodal distributions of the nanodroplet sizes comparable to those of the LUVs 1/1 and LUVs 4/1 (**Supporting Information, Figure S1**).

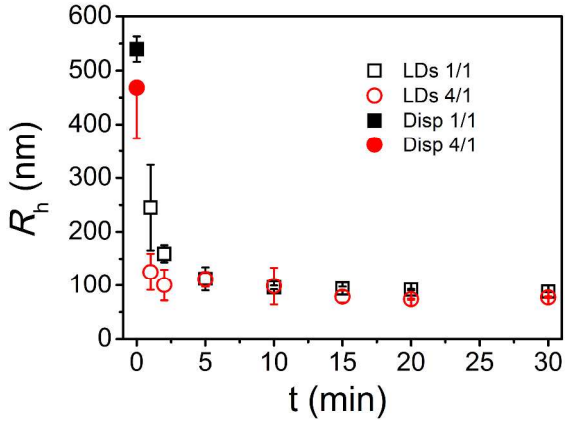

Figure 2. Effects of ultra-sonication time on dynamic-light-scattering-determined hydrodynamic radius, R_h, of SM/Chol/TOG dispersions (Disp), prepared by the modified reverse-phase evaporation method, and of lipid nanodroplets (LDs) (see **Supporting Information, Scheme S1**). Data are means ± standard deviations of five independent lipid preparations. The 1/1 and 4/1ratios indicate the theoretical molar ratios of SM and Chol. The final lipid compositions of the LDs 1/1 and LDs 4/1 were determined colorimetrically (**Table 1**).

The LDs 1/1 and 4/1, and LUVs 1/1 and 4/1 were reanalyzed in terms of their size distribution, shape, and ζ-potential, and the orientational order of the interfacial water molecules, using asymmetrical flow field flow fractionation-multi-angle light scattering (AF4-MALS) technique, TEM, DLS, and second harmonic scattering (SHS), respectively.

The DLS-estimated polydispersity (PI) ranged from ~0.1 to 0.12 for both the LDs and LUVs, which suggested that there were monodispersed particles with relatively narrow distributions of hydrodynamic radius, R_h. Separation of the LDs and LUVs by AF4-MALS and closer inspection of the resulting fractograms (**Figure 3**) confirmed monomodal distributions for these LD and LUV populations. Of note, both R_h and R_g for the LDs prepared by ultrasonication were smaller

than those for the extruded LUVs. For the LDs, R_g was smaller than R_h, while for the LUVs, R_g and R_h were very similar (**Table 2**).

Table 2. Hydrodynamic radius (R_h), radius of gyration (R_g), shape factor ρ (R_g/R_h), sphere radius (R_{TEM}), polydispersity (PI) and ζ-potential for LDs and LUVs determined by dynamic light scattering (R_h), asymmetrical flow field flow fractionation-multi-angle light scattering (R_g), transmission electron microscopy (R_{TEM}), first and second cumulants (polydispersity), and Zetasizer (ζ-potential).

Lipid preparation	R_h (nm) (mean ± s.d., n=5)	R_g (nm) (mean ± s.d., n=3)	R_g/R_h	R_{TEM} (nm) (mean ± s.d., n=35)	PI	ζ-potential (mV) n=3
LDs 1/1	55.0 ± 3.4	45.0 ± 2.7	0.82	77 ± 21	0.104	-5 ± 4
LDs 4/1	53.5 ± 5.1	42.3 ± 2.5	0.79	62 ± 14	0.117	-7 ± 8
LUVs 1/1	77.2 ± 4.5	74.1 ± 3.1	0.96	72 ± 12	0.112	-5 ± 3
LUVs 4/1	79.2 ± 3.5	76.8 ± 3.0	0.97	79 ± 18	0.112	-6 ± 7

Where indicated, data are means ± standard deviation.

The shape factor, ρ (R_g/R_h), for the LDs 1/1 and LDs 4/1 was approximately 0.8, and for the LUVs 1/1 and LUVs 4/1 was close to 1.0; these are similar to reports.[34-35] The different values of the shape factor depended on the mean segment in-particle density, which suggested different internal structures of the particles examined.[55] Based on the characteristic theoretical value of 0.775 for a homogeneous sphere and 1.0 for a spherical shell structure[56], these observed ρ values therefore suggested that the LDs had a spherical structure of uniform density throughout,

whereas the LUVs had a spherical shell structure with a lower density in the interior, and probably without a substantial solvation layer contributing to their hydrodynamic radius.

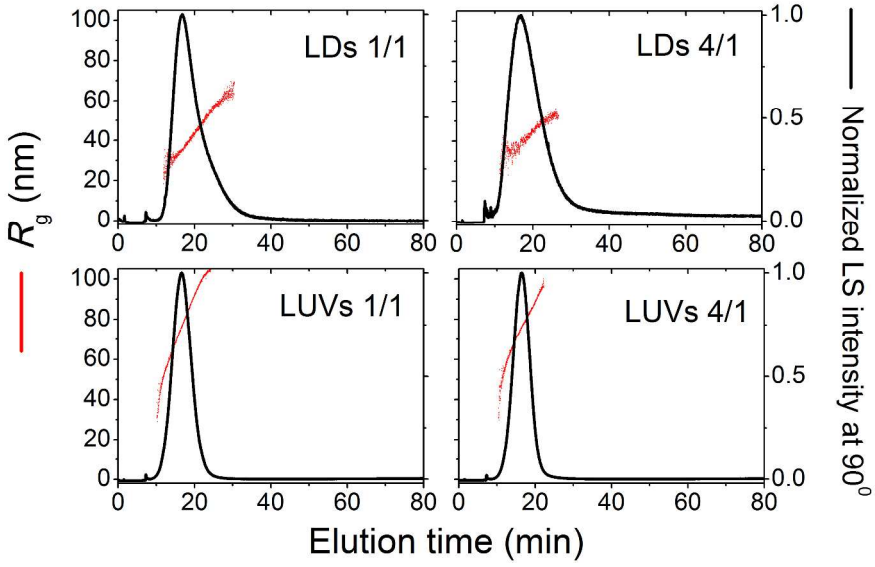

Figure 3. AF4-MALS fractograms (black curves recorded at light scattering [LS] angle of 90°) and radius of gyration, R_g (red dotted curves, determined by multi-angle light scattering), as a function of elution time for LDs and LUVs. Nanoemulsion LDs composed of SM/Chol/TOG at the theoretical molar ratio of 1/1/4.7 (LDs 1/1) and 4/1/11.7 (LDs 4/1), and LUVs made of SM/Chol at the theoretical molar ratio of 1/1 and 4/1, were eluted with Buffer A (140 mM NaCl/ 20 mM Tris.HCl / 1 mM EDTA, pH 7.4) at a cross-flow rate of 0.50 mL/min – 0.09 mL/min.

The TEM imaging demonstrated that all of these LDs and LUVs were spherically shaped structures (**Supporting Information, Figure S2**). To consider possible TEM artefacts[49], the R_{TEM} values determined on the uncrowded particles were comparable to the sizes determined by DLS and AF4-MALS, and as reported previously.[34] Qualitatively, the TEM-estimated

dimensions of the LDs were in agreement with the AF4-MALS fractograms and DLS, which showed a relative broad distribution of sizes.

The LDs 1/1, 4/1 and LUVs 1/1 and 4/1 were characterized for their ζ-potentials on their slipping planes in aqueous solution (**Table 2**), and were further examined for the orientational order of the interfacial water molecules at their monolayer or bilayer surfaces. The interfacial water molecules were probed by SHS, a non-resonant, second-order nonlinear optical technique that has been used to probe the orientational order of interfacial water molecules along the surface normal.[26, 57-59] **Figure 4** shows the maximum SHS intensities for the LDs and LUVs, where the LDs 1/1s, LUVs 1/1, LDs 4/1 and LUVs 4/1 had identical SHS responses within the standard deviation of the measuremens. These data imply that all of these SM/Chol surfaces have similar orientational order of the hydration water molecules. Moreover, SHS responses for the pure hexadecane nanodroplets were also measured, to reveal the substantial differences between the surfaces of non-polar hydrophobic molecules and the SM/Chol surfaces of the LDs and LUVs exposed to the aqueous phase. In the case of hexadecane bare oil nanodroplets, the SHS intensity was substantially enhanced due to charge-induced interfacial water ordering from the phenomenological negative charge at the surface of the pure oil nanodroplets.[12, 25, 60] In comparison to pure hexadecane nanodroplets, the ~ 5 times smaller SHS intensity is observed for all of the LDs and LUVs. These indicated that the SM/Chol surfaces have a minimal net surface charge that is in good agreement with the ζ-potential data (**Figure 1B**, **Table 2**). Taken together, it can be concluded that the surfaces of the LD monolayers and the LUV outer membrane leaflets are very similar in terms of surface potential, and thus of the orientational order of the water molecules at their surfaces.

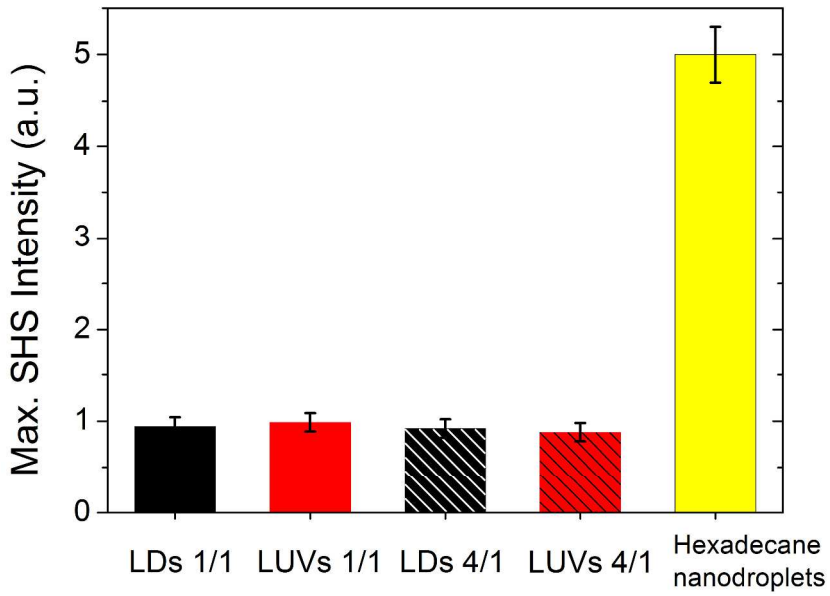

Figure 4. Orientational order of the interfacial water molecules. The SHS intensities of the tested SM/Chol/TOG lipid nanodroplets and SM/Chol large unilamellar vesicles with SM/Chol molar ratio of 1/1 (LDs 1/1 and LUVs 1/1) or SM/Chol 4/1 (LDs 4/1 and LUVs 1/1), and of pure hexadecane nanodroplets are shown, in terms of the SHS intensity at the scattering angle (35° − 45°) that gives rise to the maximum second harmonic intensity in the PPP polarization combination. This three-letter code for the polarization combination (i.e., PPP) represents the polarization of each beam from high frequency to low frequency, where P(S) refers to light polarized parallel (perpendicular) to the scattering plane. All SHS samples were prepared in 100 μM Tris-buffer, pH 7.4.

Here, the LDs 1/1 and LDs 4/1 were kinetically stable at 6 °C, 25°C , and 37 °C, as the R_h of the nanodroplets was constant even after 90 days (within experimental error) (**Supporting Information**, **Figure S4**). Moreover, the LDs were stable for at least 30 days, when prepared in the Buffer A at various pHs (7.0, 7.4, 7.8, and 8.2), and with a various NaCl concentrations (0, 70, 140, 280 mM).

Altogether, these data suggested that inclusion of the zwitterionic SM in the monolayer that shields the TOG nanodroplets reduces their ζ-potential significantly while Chol modulate this to a lesser extent. However, these surface-located amphiphilic lipids kinetically stabilize the TOG nanodroplets. Of note, lower negative values of the nanodroplet ζ-potential correlated with their higher stability, which suggested that in addition to electrostatic repulsion in terms of the electrostatic double layer, other interfacial factors have roles.[61] In particular, Chol and the methylated choline head-group of SM can significantly increase the hydration forces that contribute to repulsion between opposing membrane surfaces.[62] Another important factor that contributes to the stability of the SM/Chol-coated nanodroplets might be extensive intramolecular hydrogen bonding by the sphingosine 2-NH and 3-OH, the SM head-group phosphoryl oxygens, and the intermolecular H-bonding between SM and 3-OH of Chol in hydrated membranes.[63-65] In conclusion, the combination of SM and Chol is efficient in terms of stabilizing the LDs, and thus making them suitable for further studies. These data suggest that in terms of surface electrical characteristics, the SM/Chol surface of the LDs is very similar to that of the SM/Chol LUVs and the SUVs bilayers.

Interaction of LDs with perfringolysin O and equinatoxin II. To validate the applicability of these prepared LDs 1/1 and LDs 4/1/ in protein/lipid interaction studies, two pore-forming toxins were used: PFO and EqTx II. These proteins have already been extensively reported to interact specifically with bilayers and Langmuir monolayers that contain either Chol[40, 66-67] or SM[28, 41], respectively. Moreover, PFO can bind to the membrane only if Chol is accessible for interaction. This occurs when the Chol membrane concentrations exceeds a threshold of 30 mole% to 50 mole%, a range that can be modulated by co-existing phospholipids.[37, 68-69] This Chol threshold membrane concentration has been interpreted as a consequence of the condensing

effects of Chol or the formation of SM/Chol complexes, which is a biophysical basis for lipid rafts formation.[70-71] This phenomenon was suggested to decrease the chemical activity of Chol, i.e., providing only the accessible Chol for interactions with other molecules, including proteins.[72] The behavior of SM/Chol mixtures in bilayers and Langmuir monolayers defined our choice of the SM/Chol molar ratios of 1/1 and 4/1 to test whether the threshold Chol concentration is also relevant for the LD monolayer.

To use LDs in SPR studies, it is essential that LDs can be immobilized onto a sensor chip. We tested conditions to attach the LDs to the L1-chip, which has been regularly used for LUV immobilization.[73-74] Here, we optimized a protocol for a SPR-cycle suitable for the use of LDs (**Supporting Information, Figure S5**). These experiments demonstrated that LDs can be stably and reproducibly deposited onto the L1-chip in a similar way to LUVs, and thus can be used in SPR studies of interactions with proteins and other analytes.

Our examination of the Chol-specific PFO binding to LDs and LUVs revealed that their respective SM/Chol surfaces were very similar in terms of the Chol availability for PFO protein attachment, where only those with SM/Chol molar ratios of 1/1 bound PFO. The SPR experiments revealed comparable association/dissociation kinetics of the PFO interactions with the LDs 1/1 and LUVs 1/1, but no binding to the LDs 4/1 and LUVs 4/1 at all (**Figure 5A, B**). These data thus also reveal that a threshold Chol concentration is needed for binding of PFO to these LDs as reported for LUVs.[40, 67] The PFO interactions with the Langmuir monolayers were more complex, as these depended on both the SM/Chol molar ratio and the monolayer surface pressure. Specifically, compared to 1/1 SM/Chol monolayers, with increasing initial surface pressure, π_i, PFO detected substantially smaller increases in the 4/1 SM/Chol monolayer surface pressure, $\Delta\pi$ (**Figure 5C**). The extrapolated values of the π_i of < 20 mN/m for the SM/Chol 4/1

and ~ 33 mN/m for the SM/Chol 1/1 monolayer defined the values where PFO did not bind to the respective monolayer, which reflected the greater extent of adsorption/insertion of PFO in the SM/Chol 1/1 monolayer. Of note, the binding of PFO to the SM/Chol 4/1 monolayer (**Figure 5C**) was not in line with the inertness of PFO towards the LUVs 4/1and LDs 4/1 (**Figure 5A, B**). The changes in $\Delta\pi$ seen for the SM/Chol 4/1 monolayer might be accounted for by the relatively higher accessibility of Chol for PFO in the SM/Chol 4/1 monolayer at π_i values bellow 20 mN/m, where the monolayer was more expanded, as compared to vesicle bilayers with a lateral pressure of 30 mN/m to 35 mN/m.[75] However, another reason might be non-specific adsorption of PFO to the interphase as reported previously.[66] Additionally, these binding data suggested that the surface pressure of the SM/Chol monolayers on the LDs might be close to the lateral pressures that are typical of lipid vesicles as reported previously.[75] In summary here, these data support the view that the surface structure of the SM/Chol monolayer that surrounds the TOG core is dependent on the specific SM/Chol molar ratio, and it is similar to the surface of LUVs bilayers and Langmuir monolayesr at comparable SM/Chol molar ratios. Moreover, the Chol threshold observed for SM/Chol monolayer of the LDs suggested that the condensing effect of Chol that resulted in co-existing liquid ordered and liquid disordered lipid phases is common to the SM/Chol bilayer and monolayer, including that of the LDs. This suggestion is supported by the observation on various lipid phases in milk fat globules[76] and in monolayers prepared from their lipid extracts.[77]

The association/dissociation kinetics of EqTx II binding to the LDs and LUVs were similar (**Supporting Information, Figure S6**). The slightly slower association of EqTx II with LDs is most likely accounted for by proportionally less membrane SM in the total mass of the deposited LDs, compared to LUVs, with both loaded up to 9 kRU to 10 kRU. Similar kinetics of the EqTx

II interaction with both the LDs and LUVs reflect a similar surface location and conformation of SM molecules in LD monolayesr and LUVs bilayers. In both cases, the SM phosphoryl choline head-group should be exposed to the water phase, which will allow interactions with EqTx II.[41] We have shown previously that EqTx II interacts with SM-containing Langmuir monolayers[28], as also reported in detail for some other actinoporins, too.[78]

We used TEM as an independent method to confirm EqTx II and PFO binding to the SM/Chol surfaces and to provide structural details. As expected the dimensions of the 20-kDa EqTx II molecule and the oligomers formed were below the resolution limit of the TEM imaging (data not shown). However, it was possible to visualize larger PFO structures on the LUVs 1/1 and the SM/Chol 1/1 Langmuir monolayer LDs 1/1 and also on the LDs 1/1. In contrast, PFO structures were not seen on surfaces with a SM/Chol ratio of 4/1; i.e., LDs 4/1 and LUVs 4/1. This is in agreement with the binding data presented in **Figure 5**. As shown previously for PFO [79-81] and other Chol-dependent cytolysin structures on vesicles[82-86], PFO formed arc-like and circular oligomers with diameters that varied from 20 nm to 40 nm on the surface of the LUVs 1/1, but also on the LDs 1/1 (**Figure 6**). In addition, we transferred the SM/Chol 1/1 Langmuir monolayer with adsorbed PFO oligomers to the carbon-coated grid for visualization with TEM (**Supporting Information**, **Figure S7**). Very recently, ring and arc-like structures of a Chol-dependent cytolysin, intermedilysin, on a Langmuir monolayer were imaged by TEM[84], thus demonstrating applicability of TEM for imaging of larger proteins adsorbed or inserted into Langmuir lipid monolayers.

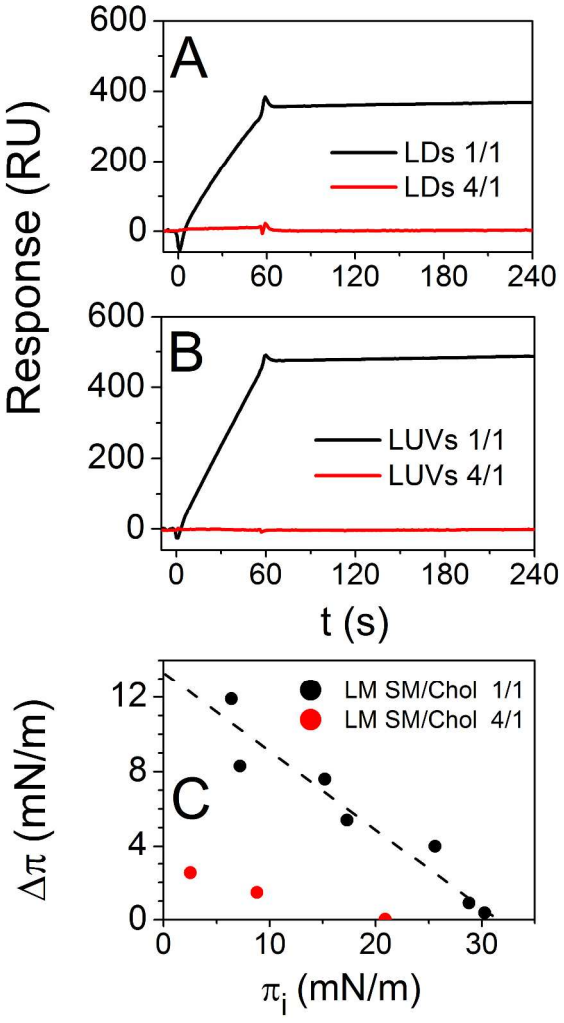

Figure 5. Binding of perfringolysin O to SM/Chol surfaces of nanoemulsion lipid nanodroplets, large unilamellar vesicles (LUVs) and Langmuir monolayers (LMs). Representative SPR-sensorgrams for binding of 500 nM perfringolysin O, using a flow rate of 10 μL/min, to LDs 1/1 and LDs 4/1 (A), and large unilamellar vesicles LUVs 1/1 and LUVs 4/1 (B), captured on the L1 sensor chip. (C) Langmuir monolayers LM SM/Chol 1/1 and LM SM/Chol 4/1 were formed on the Buffer A sub-phase at room temperature. Stable monolayers at varied initial surface pressure (π_i) were exposed to 500 nM PFO injected into the sub-phase, and increases in surface pressure ($\Delta\pi$) were monitored for at least 30 min.

The imaged PFO structures (**Figure 6**; **Supporting Information**, **Figure S7**) suggested that PFO can form very similar arc-like and completed ring-like oligomers on all of the varied membrane surfaces that include Chol levels that exceed its threshold concentration. As reported for several cholesterol-dependent cytolysins, their oligomeric ring-like structures might be pores that span the lipid bilayer, or pre-pores that sit on the protein-exposed lipid leaflet[87]. Although PFO prepores only might be expected to only form on LDs, cryogenic-TEM will be needed to analyze the observed ring-like structures in detail.

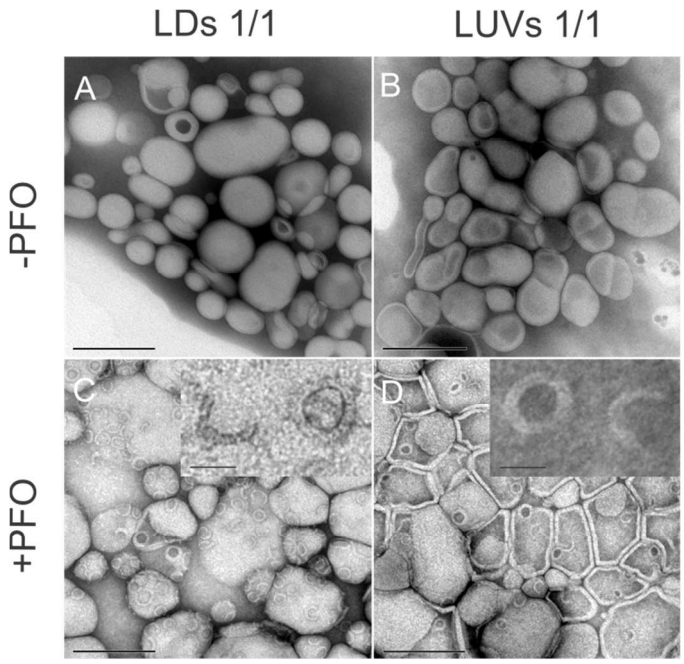

Figure 6. Transmission electron microscopy images of perfringolysin O (PFO) adsorbed onto LDs 1/1 and LUVs 1/1. (A, C) LDs composed of sphingomyelin/cholesterol/trioleoylglycerol (1/1/4.7; theoretical molar ratio) without (-PFO) or treated with (+PFO) 500 nM PFO, respectively. (B, D) LUVs of sphingomyelin/cholesterol (1/1, theoretical molar ratio) without and with 500 nM PFO. Uranyl acetate (1%, w/v) was used as a stain. Note the arcs and circles formed by PFO in (C, D). Scale bars, 200 nm; inset bar, 20 nm.

SUMMARY AND CONCLUSIONS

Our intention here was to evolve a simple and reproducible protocol for small-scale preparation of SM/Chol-coated triglyceride nanodroplets as a relatively stable biomimetic system. Such LDs will be applicable in biochemical and biophysical studies of sphingomyelin- and cholesterol-containing monolayers coupled to a hydrophobic core as pertains for intracellular lipid droplets and extracellular proteo-lipidic bodies; i.e., density lipoproteins or milk fat bodies.

In contrast to unsaturated glycerophosphatides, SMs and Chol are more difficult to be included quantitatively in artificial lipid systems, due to their higher melting temperature, the limited solubility of Chol in phospholipids, their de-mixing in membranes, the formation of Chol crystallites, and the tendency of these lipids to form non-lamellar structures. As a result, the lipid recovery can be poor and their actual molar ratios might deviate significantly from desired theoretical values. Therefore, final lipid preparations should be analyzed for the content of their individual lipid components. Moreover, we suggest that in further optimization of the protocol, both careful size determination of prepared LDs and measurement of ζ-potential changes *vs.* lipid composition might be helpful in the search for the correct amphiphilic lipid(s)/oil molar or weight ratios, to satisfy an optimal LD surface/core mass ratio, and thus reduce the contamination of LDs with excessive lipid lamellar or non-lamellar structures.

Combined SM and Chol are shown here to be efficient surfactants for the production of kinetically stable nanoemulsions of trioleoylglycerol nanodroplets. Characterization of the LD surfaces in parallel with the LUVs, and Langmuir monolayers with similar SM/Chol compositions revealed that their external surfaces that face the water phase share similar electrostatics, orientational order of the interfacial water molecules, and SM/Chol lateral organization, as probed by the SM-binding and Chol-binding proteins. It is also evident that the

Chol threshold for PFO binding seen with the SM/Chol bilayer membranes is reproduced in the SM/Chol monolayer of the LDs.

Finally, we can conclude that the modified reverse-phase evaporation and ultra-sonication of the resulting lipid dispersion allow for preparation of stable SM/Chol/TOG LDs. We suggest that this protocol is generic for preparation of LDs with desired combinations of other membrane amphiphilic lipids and non-polar lipids such as triglycerides and sterol esters, or even other non-polar synthetic liquids.

AUTHOR INFORMATION

Corresponding Author

*E-mail: peter.macek@bf.uni-lj.si

Author Contributions

V.V. prepared and characterized the LDs and LUVs, collected data and prepared figures. V.V. and V.H. provided SPR data. S.S. performed AF4-MALS experiments. H.I.O., V.V., and C.L.Y. performed SHS experiments, M. T.-Ž. performed TEM imaging. V.V. and P.M. wrote the manuscript, which was read, reviewed and approved by all of the authors. E.Ž., K.K., K.S., S.R., and P.M. designed and supervised the study.

The manuscript was written through contributions of all authors. All authors have given approval to the final version of the manuscript.

Notes

The authors declare no competing interest.

ACKNOWLEDGMENT

The Slovenian researchers were supported by the Slovenian Research Agency (grants P2-0145, P1-0184, P1-0201, J4-7162, and P1-0207). V.V. was a recipient of an EMBO Short Term Fellowship and WFS National Scholarship. H.I.O, C.L., and S.R. thank the European Research Council (grant no. 616305) for support. We thank S. Rezelj and G. Anderluh from the National Institute of Chemistry (Ljubljana, Slovenia) for supplies of recombinant perfringolysin O. The authors gratefully acknowledge Dr. Christopher Berrie for critical reading and appraisal of the manuscript.

ABBREVIATIONS

AF4, asymmetrical flow field flow fractionation; Chol, cholesterol; EDTA, ethylenediaminetetraacetic acid; DLS, dynamic light scattering; LDs, lipid nanodroplets; LUVs, large unilamellar vesicles; MALS, multi-angle light scattering; R_g, radius of gyration; R_h, hydrodynamic radius; SHS, second harmonic spectroscopy; SM, sphingomyelin; SPR, surface plasmon resonance; SUVs, small unilamellar vesicles; TEM, transmission electron microscopy; TOG, trioleoylglycerol; Tris, tris(hydroxymethyl)aminomethane.

ASSOCIATED CONTENT

Supporting Information

Preparation of unilamellar vesicles and nanoemulsion lipid nanodroplets and flowchart (**Scheme S1**), characterization of nanodroplets (**Table S1**), hydrodynamic radii (R_h) distribution of nanoemulsion lipid nanodroplets and large unilamellar vesicles determined by DLS (**Figure S1**), relationship between lipid molar fractions and geometrical radii of nanodroplets (**Figure S2**), TEM images of lipid nanodroplets and vesicles (**Figure S3**), long-term size stability of nanodroplets (**Figure S4**), surface plasmon resonance spectroscopy of nanodroplets (**Figure S5**), and binding of equinatoxin II nanodroplets and vesicles (**Figure S6**), TEM imaging of perfringolysin O adsorbed to Langmuir lipid monolayer at varied surface pressure (**Figure S7**).

REFERENCES

1. Segrest, J. P.; Jones, M. K.; De Loof, H.; Dashti, N., Structure of apolipoprotein B-100 in low density lipoproteins. *Journal of Lipid Research* **2001,** *42* (9), 1346-1367.
2. Tauchi-Sato, K.; Ozeki, S.; Houjou, T.; Taguchi, R.; Fujimoto, T., The Surface of Lipid Droplets Is a Phospholipid Monolayer with a Unique Fatty Acid Composition. *Journal of Biological Chemistry* **2002,** *277* (46), 44507-44512.
3. Hoofnagle, A. N.; Heinecke, J. W., Lipoproteomics: using mass spectrometry-based proteomics to explore the assembly, structure, and function of lipoproteins. *Journal of Lipid Research* **2009,** *50* (10), 1967-1975.
4. Thiam, A. R.; Farese Jr, R. V.; Walther, T. C., The biophysics and cell biology of lipid droplets. *Nat Rev Mol Cell Biol* **2013,** *14* (12), 775-786.
5. Ben M'barek, K.; Ajjaji, D.; Chorlay, A.; Vanni, S.; Forêt, L.; Thiam, A. R., ER Membrane Phospholipids and Surface Tension Control Cellular Lipid Droplet Formation. *Developmental Cell 41* (6), 591-604.e7.
6. Miller, K. W.; Small, D. M., Triolein-cholesteryl oleate-cholesterol-lecithin emulsions: structural models of triglyceride-rich lipoproteins. *Biochemistry* **1983,** *22* (2), 443-451.
7. Saito, H.; Nishiwaki, K.; Handa, T.; Ito, S.; Miyajima, K., Comparative Study of Fluorescence Anisotropy in Surface Monolayers of Emulsions and Bilayers of Vesicles. *Langmuir* **1995,** *11* (10), 3742-3747.

8. Bricarello, D. A.; Smilowitz, J. T.; Zivkovic, A. M.; German, J. B.; Parikh, A. N., Reconstituted Lipoprotein: A Versatile Class of Biologically-Inspired Nanostructures. *ACS Nano* **2011,** *5* (1), 42-57.
9. Wang, Y.; Zhou, X.-M.; Ma, X.; Du, Y.; Zheng, L.; Liu, P., Construction of Nanodroplet/Adiposome and Artificial Lipid Droplets. *ACS Nano* **2016,** *10* (3), 3312-3322.
10. Okur, H. I.; Chen, Y.; Smolentsev, N.; Zdrali, E.; Roke, S., Interfacial Structure and Hydration of 3D Lipid Monolayers in Aqueous Solution. *J Phys Chem B* **2017,** *121* (13), 2808-2813.
11. Mirheydari, M.; Mann, E. K.; Kooijman, E. E., Interaction of a model apolipoprotein, apoLp-III, with an oil-phospholipid interface. *Biochim Biophys Acta* **2018,** *1860* (2), 396-406.
12. Chen, Y.; Jena, K. C.; Lütgebaucks, C.; Okur, H. I.; Roke, S., Three Dimensional Nano "Langmuir Trough" for Lipid Studies. *Nano Letters* **2015,** *15* (8), 5558-5563.
13. Chen, Y.; Okur, H. I.; Lütgebaucks, C.; Roke, S., Zwitterionic and Charged Lipids Form Remarkably Different Structures on Nanoscale Oil Droplets in Aqueous Solution. *Langmuir* **2018,** *34* (3), 1042-1050.
14. Mouritsen, O. G., Model Answers to Lipid Membrane Questions. *Cold Spring Harbor Perspectives in Biology* **2011,** *3* (9).
15. Sezgin, E.; Levental, I.; Grzybek, M.; Schwarzmann, G.; Mueller, V.; Honigmann, A.; Belov, V. N.; Eggeling, C.; Coskun, Ü.; Simons, K.; Schwille, P., Partitioning, diffusion, and ligand binding of raft lipid analogs in model and cellular plasma membranes. *Biochimica et Biophysica Acta (BBA) - Biomembranes* **2012,** *1818* (7), 1777-1784.
16. Blume, A.; Kerth, A., Peptide and protein binding to lipid monolayers studied by FT-IRRA spectroscopy. *Biochimica et Biophysica Acta (BBA) - Biomembranes* **2013,** *1828* (10), 2294-2305.
17. Czogalla, A.; Grzybek, M.; Jones, W.; Coskun, Ü., Validity and applicability of membrane model systems for studying interactions of peripheral membrane proteins with lipids. *Biochimica et Biophysica Acta (BBA) - Molecular and Cell Biology of Lipids* **2014,** *1841* (8), 1049-1059.
18. Elderdfi, M.; Sikorski, A. F., Langmuir-Monolayer Methodologies for Characterizing Protein-Lipid Interactions. *Chemistry and Physics of Lipids* **2018**.
19. Bartz, R.; Li, W.-H.; Venables, B.; Zehmer, J. K.; Roth, M. R.; Welti, R.; Anderson, R. G. W.; Liu, P.; Chapman, K. D., Lipidomics reveals that adiposomes store ether lipids and mediate phospholipid traffic. *Journal of Lipid Research* **2007,** *48* (4), 837-847.
20. Prassl, R.; Laggner, P., Molecular structure of low density lipoprotein: current status and future challenges. *Eur Biophys J* **2009,** *38* (2), 145-58.
21. Wiesner, P.; Leidl, K.; Boettcher, A.; Schmitz, G.; Liebisch, G., Lipid profiling of FPLC-separated lipoprotein fractions by electrospray ionization tandem mass spectrometry. *Journal of Lipid Research* **2009,** *50* (3), 574-585.
22. Quinn, P. J.; Wolf, C., The liquid-ordered phase in membranes. *Biochimica et Biophysica Acta (BBA) - Biomembranes* **2009,** *1788* (1), 33-46.
23. Lingwood, D.; Simons, K., Lipid Rafts As a Membrane-Organizing Principle. *Science* **2010,** *327* (5961), 46-50.
24. Sezgin, E.; Levental, I.; Mayor, S.; Eggeling, C., The mystery of membrane organization: composition, regulation and roles of lipid rafts. *Nat Rev Mol Cell Biol* **2017,** *advance online publication*.

25. Zdrali, E.; Chen, Y.; Okur, H. I.; Wilkins, D. M.; Roke, S., The Molecular Mechanism of Nanodroplet Stability. *ACS Nano* **2017,** *11* (12), 12111-12120.
26. Roke, S.; Gonella, G., Nonlinear Light Scattering and Spectroscopy of Particles and Droplets in Liquids. *Annual Review of Physical Chemistry* **2012,** *63* (1), 353-378.
27. Smolentsev, N.; Lütgebaucks, C.; Okur, H. I.; de Beer, A. G. F.; Roke, S., Intermolecular Headgroup Interaction and Hydration as Driving Forces for Lipid Transmembrane Asymmetry. *Journal of the American Chemical Society* **2016,** *138* (12), 4053-4060.
28. Hong, Q.; Gutiérrez-Aguirre, I.; Barlič, A.; Malovrh, P.; Kristan, K.; Podlesek, Z.; Maček, P.; Turk, D.; Gonzáles-Mañas, J. M.; Lakey, J. H.; Anderluh, G., Two-step membrane binding by Equinatoxin II, a pore-forming toxin from the sea anemone, involves an exposed aromatic cluster and a flexible helix. *J Biol Chem* **2002,** *277* (44), 41916-24.
29. Szoka, F.; Olson, F.; Heath, T.; Vail, W.; Mayhew, E.; Papahadjopoulos, D., Preparation of unilamellar liposomes of intermediate size (0.1–0.2 μm) by a combination of reverse phase evaporation and extrusion through polycarbonate membranes. *Biochimica et Biophysica Acta (BBA) - Biomembranes* **1980,** *601*, 559-571.
30. Moscho, A.; Orwar, O.; Chiu, D. T.; Modi, B. P.; Zare, R. N., Rapid preparation of giant unilamellar vesicles. *Proc.Natl.Acad.Sci.USA* **1996,** *93*, 11443-11447.
31. Provencher, S. W., CONTIN: A general purpose constrained regularization program for inverting noisy linear algebraic and integral equations. *Computer Physics Communications* **1982,** *27* (3), 229-242.
32. Sitar, S.; Aseyev, V.; Kogej, K., Differences in association behavior of isotactic and atactic poly(methacrylic acid). *Polymer* **2014,** *55* (3), 848-854.
33. Sitar, S.; Aseyev, V.; Kogej, K., Microgel-like aggregates of isotactic and atactic poly(methacrylic acid) chains in aqueous alkali chloride solutions as evidenced by light scattering. *Soft Matter* **2014,** *10* (39), 7712-7722.
34. Vezočnik, V.; Rebolj, K.; Sitar, S.; Ota, K.; Tušek-Žnidarič, M.; Štrus, J.; Sepčić, K.; Pahovnik, D.; Maček, P.; Žagar, E., Size fractionation and size characterization of nanoemulsions of lipid droplets and large unilamellar lipid vesicles by asymmetric-flow field-flow fractionation/multi-angle light scattering and dynamic light scattering. *Journal of Chromatography A* **2015,** *1418*, 185-191.
35. Sitar, S.; Vezocnik, V.; Macek, P.; Kogej, K.; Pahovnik, D.; Zagar, E., Pitfalls in Size Characterization of Soft Particles by Dynamic Light Scattering Online Coupled to Asymmetrical Flow Field-Flow Fractionation. *Anal Chem* **2017,** *89* (21), 11744-11752.
36. Rossjohn, J.; Feil, S. C.; McKinstry, W. J.; Tweten, R. K.; Parker, M. W., Structure of a cholesterol-binding, thiol-activated cytolysin and a model of its membrane form. *Cell* **1997,** *89*, 685-692.
37. Heuck, A. P.; Hotze, E. M.; Tweten, R. K.; Johnson, A. E., Mechanism of membrane insertion of a multimeric β-barrel protein. Perfringolysin O creates a pore using ordered and coupled conformational changes. *Mol.Cell* **2000,** *6*, 1233-1242.
38. Tweten, R. K., Cholesterol-Dependent Cytolysins, a Family of Versatile Pore-Forming Toxins. *Infection and Immunity* **2005,** *73* (10), 6199-6209.
39. Nelson, L. D.; Johnson, A. E.; London, E., How Interaction of Perfringolysin O with Membranes Is Controlled by Sterol Structure, Lipid Structure, and Physiological Low pH. *Journal Of Biological Chemistry* **2008,** *283* (8), 4632-4642.
40. Johnson, B. B.; Heuck, A. P., Perfringolysin O Structure and Mechanism of Pore Formation as a Paradigm for Cholesterol-Dependent Cytolysins. In *MACPF/CDC Proteins* -

Agents of Defence, Attack and Invasion, Anderluh, G.; Gilbert, R., Eds. Springer Netherlands: Dordrecht, 2014; pp 63-81.
41. Rojko, N.; Dalla Serra, M.; Maček, P.; Anderluh, G., Pore formation by actinoporins, cytolysins from sea anemones. *Biochimica et Biophysica Acta (BBA) - Biomembranes* **2016,** *1858* (3), 446-456.
42. Kishimoto, T.; Ishitsuka, R.; Kobayashi, T., Detectors for evaluating the cellular landscape of sphingomyelin- and cholesterol-rich membrane domains. *Biochim Biophys Acta* **2016,** *1861* (8 Pt B), 812-29.
43. Patil, Y. P.; Jadhav, S., Novel methods for liposome preparation. *Chemistry and Physics of Lipids* **2014,** *177*, 8-18.
44. Epand, R. M.; Bach, D.; Wachtel, E., In vitro determination of the solubility limit of cholesterol in phospholipid bilayers. *Chemistry and Physics of Lipids* **2016,** *199*, 3-10.
45. Buboltz, J. T.; Feigenson, G. W., A novel strategy for the preparation of liposomes: rapid solvent exchange. *Biochimica et Biophysica Acta: Bio-Membranes* **1999,** *1417* (2), 232-245.
46. Veatch, S. L.; Keller, S. L., Separation of Liquid Phases in Giant Vesicles of Ternary Mixtures of Phospholipids and Cholesterol. *Biophysical Journal* **2003,** *85* (5), 3074-3083.
47. Mason, T. G.; Wilking, J. N.; Meleson, K.; Chang, C. B.; Graves, S. M., Nanoemulsions: formation, structure, and physical properties. *Journal of Physics: Condensed Matter* **2006,** *18* (41), R635.
48. McClements, D. J., Critical Review of Techniques and Methodologies for Characterization of Emulsion Stability. *Critical Reviews in Food Science and Nutrition* **2007,** *47* (7), 611-649.
49. Klang, V.; Matsko, N. B.; Valenta, C.; Hofer, F., Electron microscopy of nanoemulsions: An essential tool for characterisation and stability assessment. *Micron* **2012,** *43* (2–3), 85-103.
50. Ekman, S.; Derksen, A.; Small, D. M., The partitioning of fatty acid and cholesterol between core and surfaces of phosphatidylcholine-triolein emulsions at pH 7.4. *Biochimica et Biophysica Acta (BBA) - Lipids and Lipid Metabolism* **1988,** *959* (3), 343-348.
51. Marinova, K. G.; Alargova, R. G.; Denkov, N. D.; Velev, O. D.; Petsev, D. N.; Ivanov, I. B.; Borwankar, R. P., Charging of Oil−Water Interfaces Due to Spontaneous Adsorption of Hydroxyl Ions. *Langmuir* **1996,** *12* (8), 2045-2051.
52. Vácha, R.; Rick, S. W.; Jungwirth, P.; de Beer, A. G. F.; de Aguiar, H. B.; Samson, J.-S.; Roke, S., The Orientation and Charge of Water at the Hydrophobic Oil Droplet–Water Interface. *Journal of the American Chemical Society* **2011,** *133* (26), 10204-10210.
53. Magarkar, A.; Dhawan, V.; Kallinteri, P.; Viitala, T.; Elmowafy, M.; Róg, T.; Bunker, A., Cholesterol level affects surface charge of lipid membranes in saline solution. *Scientific Reports* **2014,** *4*, 5005.
54. Delmas, T.; Piraux, H.; Couffin, A.-C.; Texier, I.; Vinet, F.; Poulin, P.; Cates, M. E.; Bibette, J., How To Prepare and Stabilize Very Small Nanoemulsions. *Langmuir* **2011,** *27* (5), 1683-1692.
55. Stauch, O.; Schubert, R.; Savin, G.; Burchard, W., Structure of Artificial Cytoskeleton Containing Liposomes in Aqueous Solution Studied by Static and Dynamic Light Scattering. *Biomacromolecules* **2002,** *3* (3), 565-578.
56. Schärtl, W., *Light Scattering from Polymer Solutions and Nanoparticle Dispersions*. Springer-Verlag Berlin Heidelberg: 2007.

57. Schurer, B.; Wunderlich, S.; Sauerbeck, C.; Peschel, U.; Peukert, W., Probing colloidal interfaces by angle-resolved second harmonic light scattering. *Physical Review B* **2010,** *82* (24), 241404.
58. Scheu, R.; Rankin, B. M.; Chen, Y.; Jena, K. C.; Ben-Amotz, D.; Roke, S., Charge Asymmetry at Aqueous Hydrophobic Interfaces and Hydration Shells. *Angewandte Chemie International Edition* **2014,** *53* (36), 9560-9563.
59. Scheu, R.; Chen, Y.; de Aguiar, H. B.; Rankin, B. M.; Ben-Amotz, D.; Roke, S., Specific Ion Effects in Amphiphile Hydration and Interface Stabilization. *Journal of the American Chemical Society* **2014,** *136* (5), 2040-2047.
60. Agmon, N.; Bakker, H. J.; Campen, R. K.; Henchman, R. H.; Pohl, P.; Roke, S.; Thämer, M.; Hassanali, A., Protons and Hydroxide Ions in Aqueous Systems. *Chemical Reviews* **2016,** *116* (13), 7642-7672.
61. Donaldson, S. H.; Røyne, A.; Kristiansen, K.; Rapp, M. V.; Das, S.; Gebbie, M. A.; Lee, D. W.; Stock, P.; Valtiner, M.; Israelachvili, J., Developing a General Interaction Potential for Hydrophobic and Hydrophilic Interactions. *Langmuir* **2015,** *31* (7), 2051-2064.
62. Rand, R. P.; Parsegian, V. A., Hydration forces between phospholipid bilayers. *Biochimica et Biophysica Acta (BBA) - Reviews on Biomembranes* **1989,** *988* (3), 351-376.
63. Matsumori, N.; Yamaguchi, T.; Maeta, Y.; Murata, M., Orientation and Order of the Amide Group of Sphingomyelin in Bilayers Determined by Solid-State NMR. *Biophysical Journal* **2015,** *108* (12), 2816-2824.
64. Sodt, Alexander J.; Pastor, Richard W.; Lyman, E., Hexagonal Substructure and Hydrogen Bonding in Liquid-Ordered Phases Containing Palmitoyl Sphingomyelin. *Biophysical Journal 109* (5), 948-955.
65. Slotte, J. P., The importance of hydrogen bonding in sphingomyelin's membrane interactions with co-lipids. *Biochimica et Biophysica Acta (BBA) - Biomembranes* **2016,** *1858* (2), 304-310.
66. Alouf, J. E.; Geoffroy, C.; Pattus, F.; Verger, R., Surface properties of bacterial sulfhydryl-activated cytolytic toxins. *European Journal of Biochemistry* **1984,** *141* (1), 205-210.
67. Flanagan, J. J.; Tweten, R. K.; Johnson, A. E.; Heuck, A. P., Cholesterol Exposure at the Membrane Surface Is Necessary and Sufficient to Trigger Perfringolysin O Binding. *Biochemistry* **2009,** *48* (18), 3977-3987.
68. Johnson, B. B.; Moe, P. C.; Wang, D.; Rossi, K.; Trigatti, B. L.; Heuck, A. P., Modifications in perfringolysin o domain 4 alter the cholesterol concentration threshold required for binding. *Biochemistry* **2012,** *51* (16), 3373-82.
69. Johnson, B. B.; Breña, M.; Anguita, J.; Heuck, A. P., Mechanistic Insights into the Cholesterol-dependent Binding of Perfringolysin O-based Probes and Cell Membranes. *Scientific Reports* **2017,** *7* (1), 13793.
70. Marquardt, D.; Kucerka, N.; Wassall, S. R.; Harroun, T. A.; Katsaras, J., Cholesterol's location in lipid bilayers. *Chem Phys Lipids* **2016,** *199*, 17-25.
71. Krause, M. R.; Regen, S. L., The Structural Role of Cholesterol in Cell Membranes: From Condensed Bilayers to Lipid Rafts. *Accounts of Chemical Research* **2014,** *47* (12), 3512-3521.
72. Lange, Y.; Tabei, S. M. A.; Ye, J.; Steck, T. L., Stability and Stoichiometry of Bilayer Phospholipid–Cholesterol Complexes: Relationship to Cellular Sterol Distribution and Homeostasis. *Biochemistry* **2013,** *52* (40), 6950-6959.

73. Anderluh, G.; Beseničar, M.; Kladnik, A.; Lakey, J. H.; Maček, P., Properties of nonfused liposomes immobilized on an L1 Biacore chip and their permeabilization by a eukaryotic pore-forming toxin. *Analytical Biochemistry* **2005,** *344* (1), 43-52.
74. Hodnik, V.; Anderluh, G., Surface Plasmon Resonance for Measuring Interactions of Proteins with Lipid Membranes. In *Lipid-Protein Interactions: Methods and Protocols*, Kleinschmidt, J. H., Ed. Humana Press: Totowa, NJ, 2013; pp 23-36.
75. Marsh, D., Lateral pressure in membranes. *Biochimica et Biophysica Acta (BBA) - Reviews on Biomembranes* **1996,** *1286* (3), 183-223.
76. Nguyen, H. T. H.; Madec, M.-N.; Ong, L.; Kentish, S. E.; Gras, S. L.; Lopez, C., The dynamics of the biological membrane surrounding the buffalo milk fat globule investigated as a function of temperature. *Food Chemistry* **2016,** *204*, 343-351.
77. Murthy, A. V. R.; Guyomarc'h, F.; Paboeuf, G.; Vié, V.; Lopez, C., Cholesterol strongly affects the organization of lipid monolayers studied as models of the milk fat globule membrane: Condensing effect and change in the lipid domain morphology. *Biochimica et Biophysica Acta (BBA) - Biomembranes* **2015,** *1848* (10, Part A), 2308-2316.
78. Pedrera, L.; Fanani, M. L.; Ros, U.; Lanio, M. E.; Maggio, B.; Alvarez, C., Sticholysin I-membrane interaction: an interplay between the presence of sphingomyelin and membrane fluidity. *Biochim Biophys Acta* **2014,** *1838* (7), 1752-9.
79. Olofsson, A.; Hebert, H.; Thelestam, M., The projection structure of perfringolysin O (Clostridium perfringens theta-toxin). *Febs Letters* **1993,** *319*, 125-127.
80. Hotze, E. M.; Wilson-Kubalek, E.; Farrand, A. J.; Bentsen, L.; Parker, M. W.; Johnson, A. E.; Tweten, R. K., Monomer-Monomer Interactions Propagate Structural Transitions Necessary for Pore Formation by the Cholesterol-dependent Cytolysins. *Journal of Biological Chemistry* **2012,** *287* (29), 24534-24543.
81. Czajkowsky, D. M.; Sun, J.; Shao, Z., Single molecule compression reveals intra-protein forces drive cytotoxin pore formation. *eLife* **2015,** *4*.
82. Tilley, S. J.; Orlova, E. V.; Gilbert, R. J.; Andrew, P. W.; Saibil, H. R., Structural basis of pore formation by the bacterial toxin pneumolysin. *Cell* **2005,** *121* (2), 247-56.
83. Mulvihill, E.; van Pee, K.; Mari, S. A.; Müller, D. J.; Yildiz, Ö., Directly observing the lipid-dependent self-assembly and pore-forming mechanism of the cytolytic toxin listeriolysin O. *Nano Letters* **2015**.
84. Boyd, C. M.; Parsons, E. S.; Smith, R. A. G.; Seddon, J. M.; Ces, O.; Bubeck, D., Disentangling the roles of cholesterol and CD59 in intermedilysin pore formation. *Scientific Reports* **2016,** *6*, 38446.
85. Ruan, Y.; Rezelj, S. a.; Bedina Zavec, A.; Anderluh, G.; Scheuring, S., Listeriolysin O Membrane Damaging Activity Involves Arc Formation and Lineaction - Implication for *Listeria monocytogenes* Escape from Phagocytic Vacuole. *PLoS Pathog* **2016,** *12* (4), e1005597.
86. van Pee, K.; Neuhaus, A.; D'Imprima, E.; Mills, D. J.; Kühlbrandt, W.; Yildiz, Ö., CryoEM structures of membrane pore and prepore complex reveal cytolytic mechanism of Pneumolysin. *eLife* **2017,** *6*, e23644.
87. Gilbert, R. J.; Mikelj, M.; Dalla Serra, M.; Froelich, C. J.; Anderluh, G., Effects of MACPF/CDC proteins on lipid membranes. *Cell Mol Life Sci* **2013,** *70* (12), 2083-98.

TOC graphic

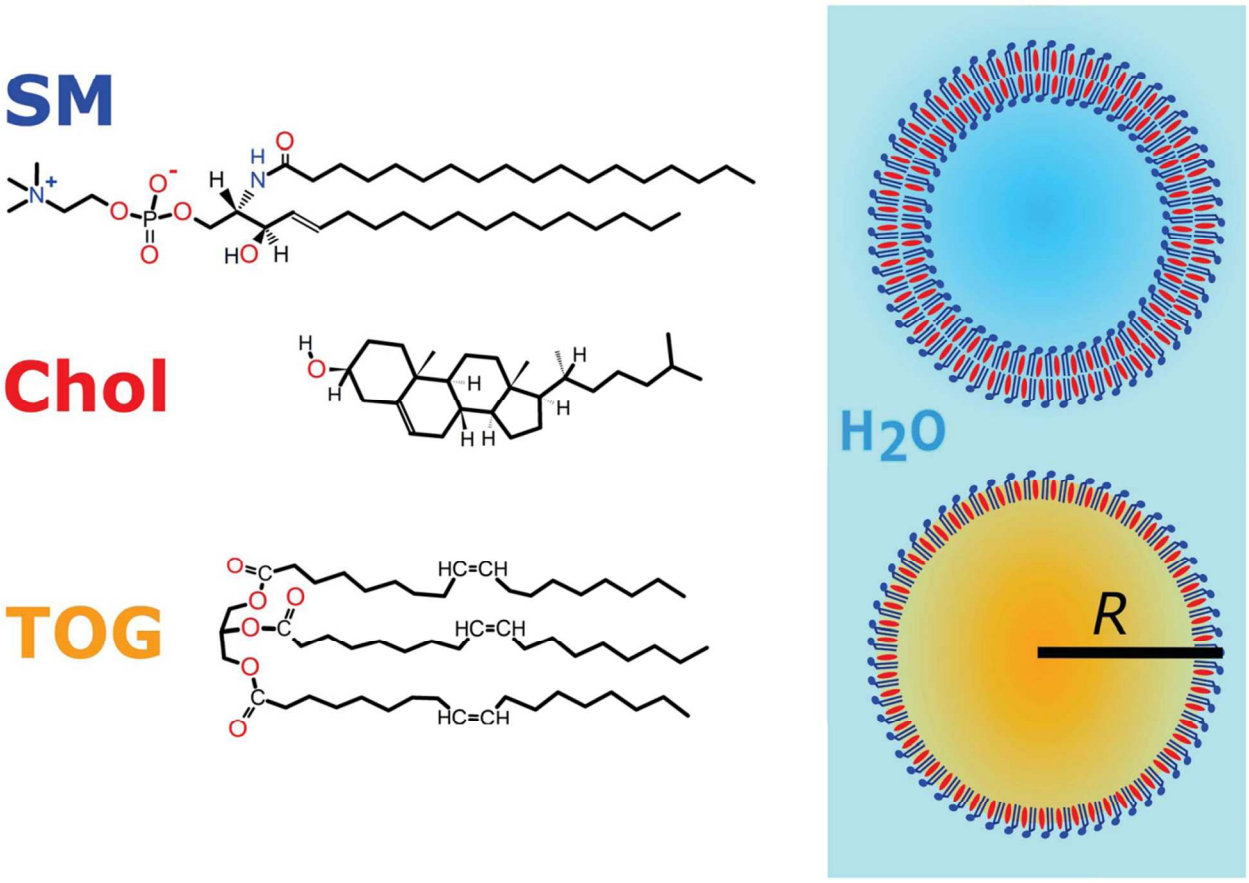

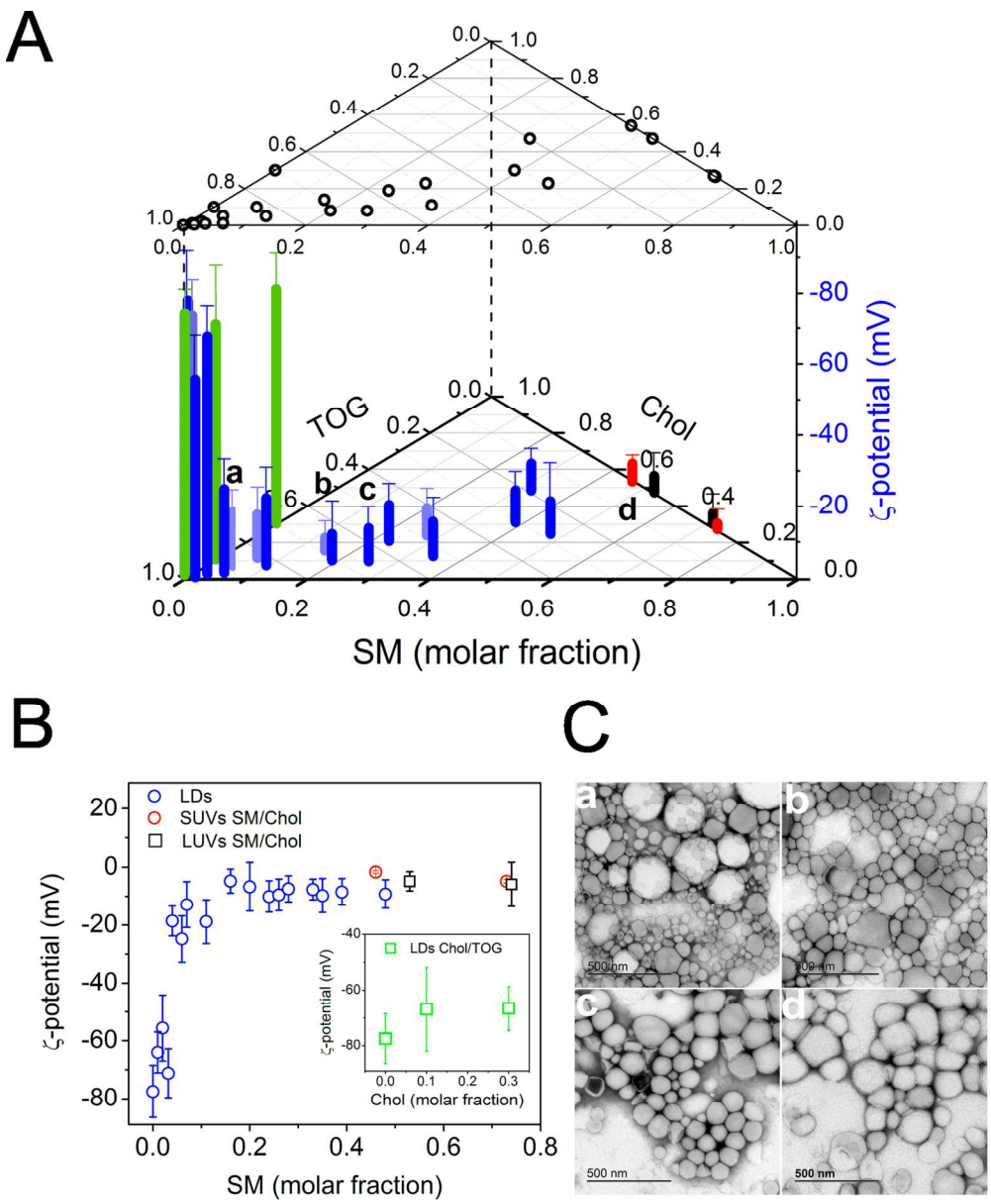

Figure 1

144x174mm (300 x 300 DPI)

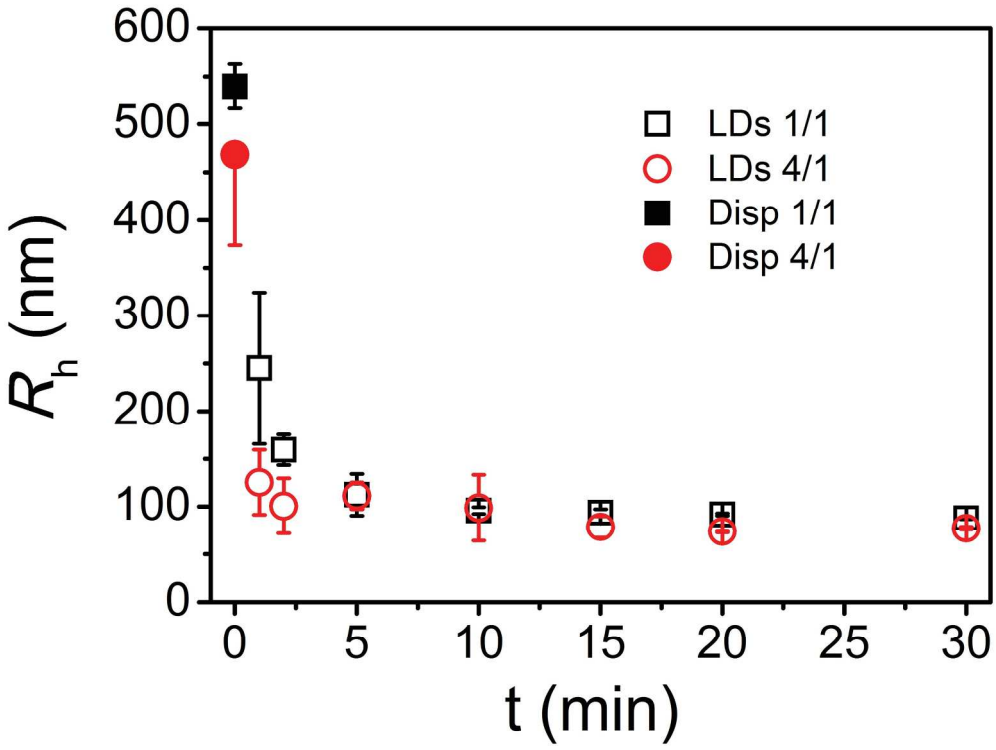

Figure 2

216x161mm (300 x 300 DPI)

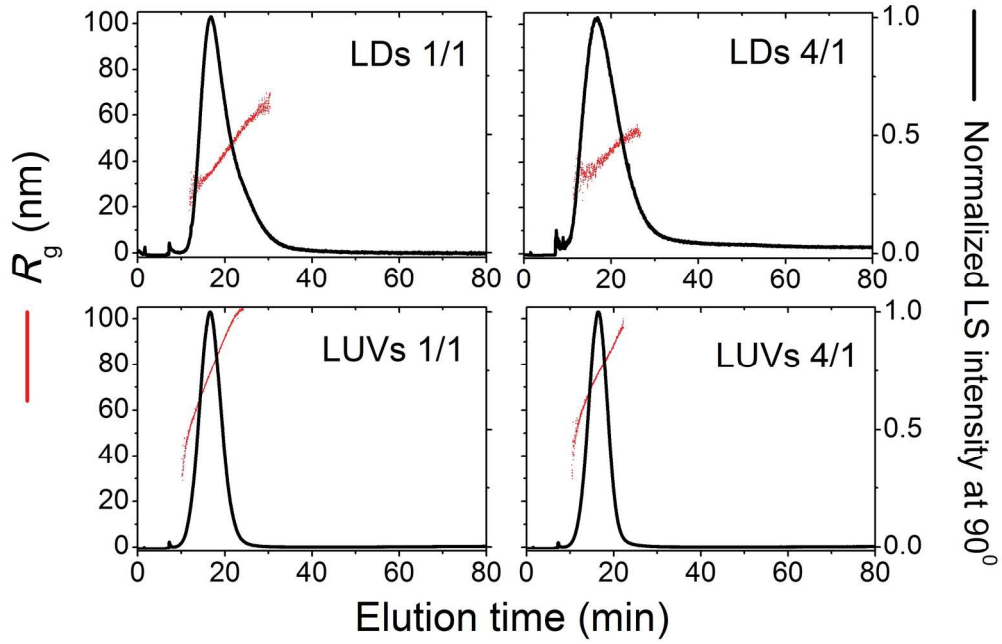

Figure 3

186x120mm (300 x 300 DPI)

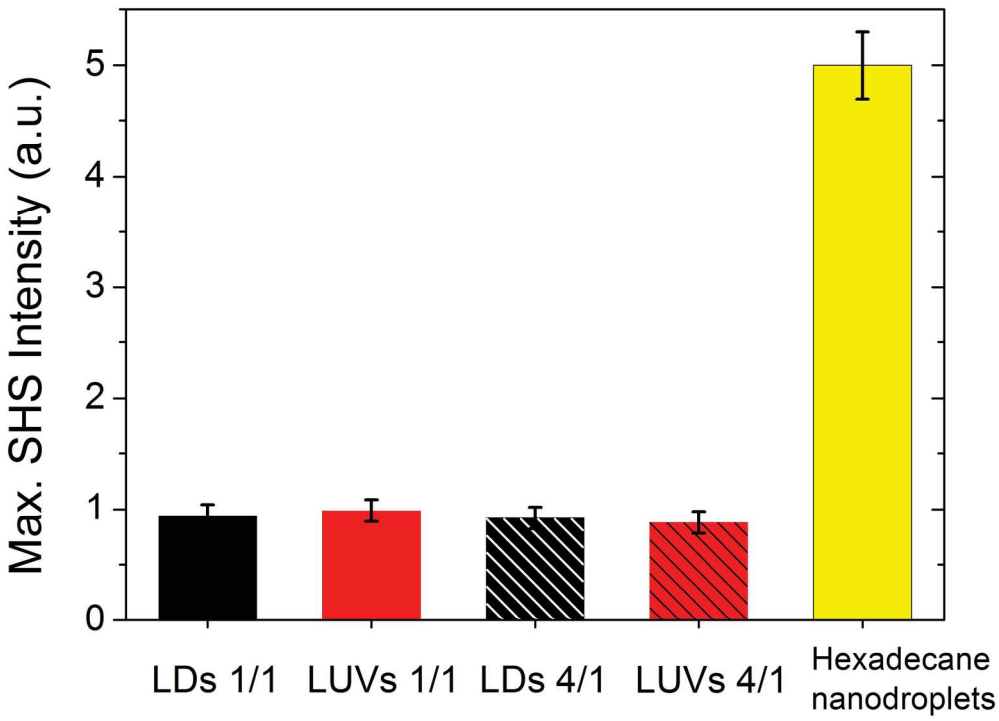

Figure 4

193x137mm (300 x 300 DPI)

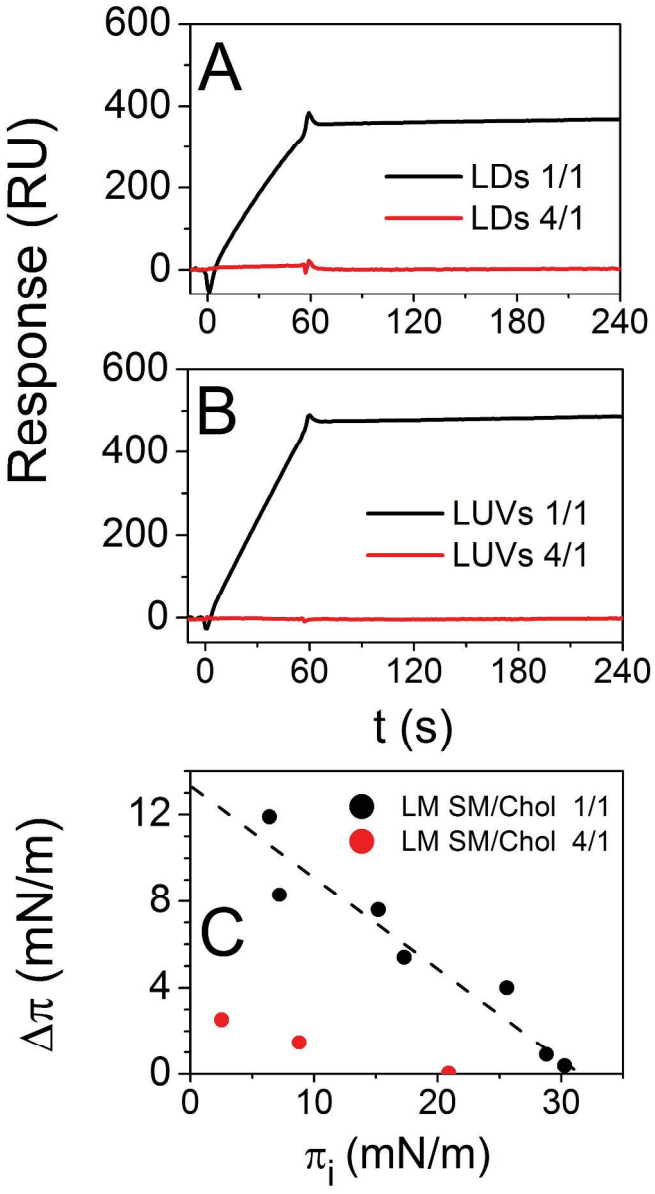

365x662mm (300 x 300 DPI)

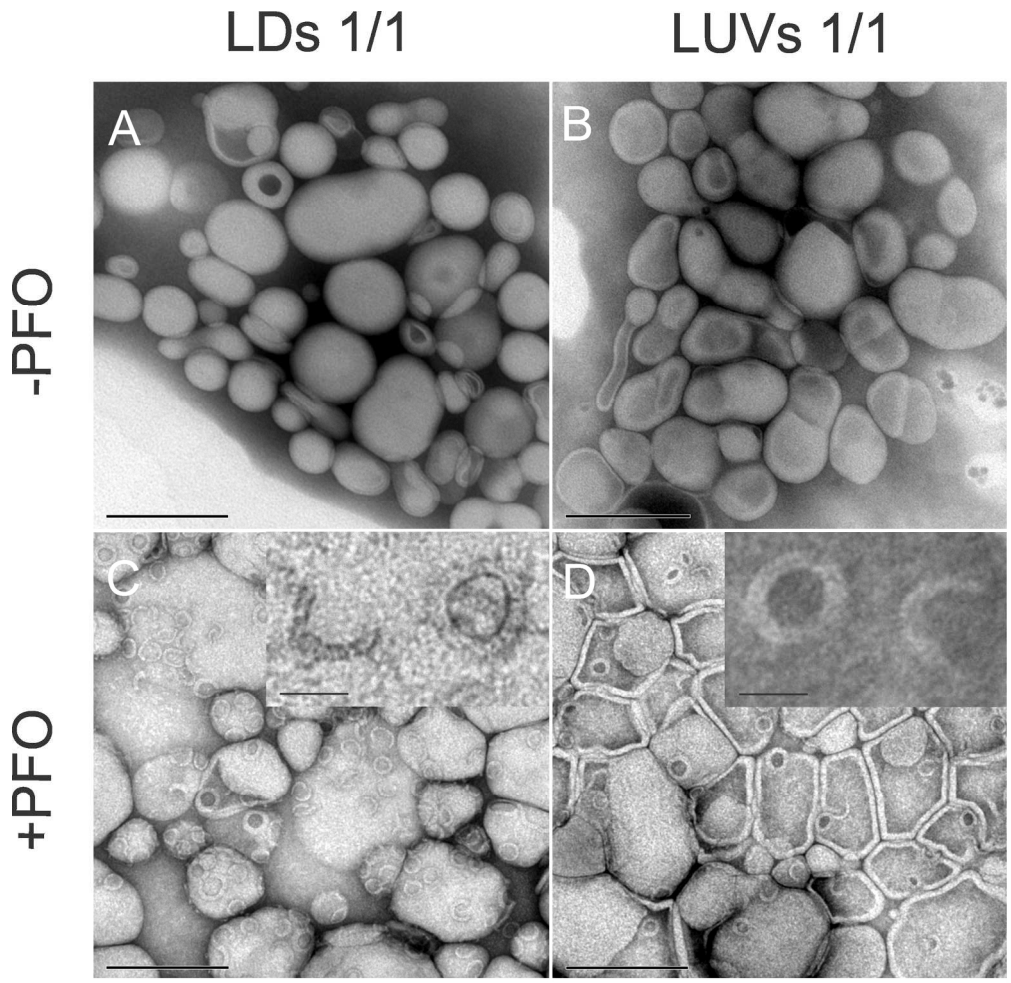

202x198mm (300 x 300 DPI)